Journal of Alloys and Compounds 722 (2017) 996–1001

Contents lists available at ScienceDirect

Journal of Alloys and Compounds

journal homepage: http://www.elsevier.com/locate/jalcom

Supersonically sprayed gas- and water-sensing MIL-100(Fe) films

Jong-Gun Lee [a, 1], Bhavana N. Joshi [a, 1], Edmund Samuel [a], Seongpil An [a], Mark T. Swihart [b], Ji Sun Lee [c], Young Kyu Hwang [c], Jong-San Chang [c, d, **], Sam S. Yoon [a, *]

[a] School of Mechanical Engineering, Korea University, Seoul, 02841, Republic of Korea
[b] Department of Chemical & Biological Engineering, University at Buffalo, The State University of New York, Buffalo, NY, 14260-4200, USA
[c] Res. Group for Nanocatalysts, Korea Res. Inst. of Chem. Tech. (KRICT), Daejeon, 34114, Republic of Korea
[d] Department of Chemistry, Sungkyunkwan University, Suwon 16419, Republic of Korea

ARTICLE INFO

Article history:
Received 13 April 2017
Received in revised form
13 June 2017
Accepted 18 June 2017
Available online 20 June 2017

Keywords:
Supersonic spraying
MIL-100
Water adsorption
Humidity sensor

ABSTRACT

Highly uniform, mechanically stable, dense, and water-adsorbing MIL-100(Fe) films were fabricated via supersonic spraying, a rapid, high-throughput, and scalable method compatible with roll-to-roll processing. The film surface area (1667 $m^2 g^{-1}$) was comparable to that of the nanoparticles from which it was prepared (2009 $m^2 g^{-1}$), and was higher than previously reported values for MIL-100(Fe) films. The gas and water adsorption abilities of the film were tested by nitrogen physisorption and water adsorption at 30 °C. The supersonically sprayed film was mechanically resistant up to a critical scratching load of 1.84 N, higher than the critical scratchability loads of dip-coated or spin-coated films. In humidity-sensing applications, films that incorporated conductive Ag nanowires were highly responsive to environmental humidity, demonstrating applicability as water vapor sensors. The fabricated films were characterized by X-ray diffraction, Raman spectroscopy, Fourier transform infrared spectroscopy, scanning electron microscopy, and atomic force microscopy.

1. Introduction

Metal organic frameworks (MOFs) are well known for their high surface areas, large pore volumes, and tunable pore sizes and crystal structures [1]. Such MOFs consist of repeated units of metal centers coupled by organic linkers. Bulk MOFs have been used for gas storage, separation, and purification, including carbon capture [2]. Production of MOF thin films is essential for many practical applications, including membrane separations, catalysis, sensing, energy conversion, optics and microelectronics [3,4], and heat pumps [5].

The mesoporous Materials of Institute Lavoisier (MIL)-100 and −101 are members of a family of MOFs based on trivalent metals linked with carboxylate ligands, as first reported by Ferey et al. [6]. MIL-100(Fe) contains iron as the metal and benzene-tricarboxylate (BTC) molecules as the organic linkers, and is known for its low toxicity [7]. Its structure includes two mesoporous cages of 25 and 29 Å in size accessible via micropore windows of 5 and 9 Å [8]. Most MOFs have limited hydrothermal stability. However, MIL-100(Fe) has both high hydrothermal stability and a large water adsorption capacity [9]. Moreover, it shows the unusual phenomenon of reversible water adsorption and the capability to regenerate the hydrated framework below 70 °C, through formation of weakly hydrogen-bonded molecules [10]. Accordingly, highly porous MIL-100(Fe) has been considered as a potential water adsorbent for energy-efficient dehumidification and adsorptive heat transformation applications [9,10].

In recent years, numerous researchers have attempted to fabricate films of MIL-100 series MOFs. Campagnol et al. reported the use of MIL-100(Fe) thin films with surface areas of 722 $m^2 g^{-1}$ fabricated by electrochemical synthesis [11] for antifouling, gas separation, and vapor separation applications. Marquez et al. [3] reported the fabrication of transparent thin films of MIL-100 by dip-coating, using a dispersion of MIL-100 nanoparticles. Other than MIL-100, electrochemically synthesized Cu-BTC films were reported by Ameloot et al. for water adsorption [12]. Demessence

* Corresponding author.
** Corresponding author. Res. Group for Nanocatalysts, Korea Res. Inst. of Chem. Tech. (KRICT), Daejeon, 34114, Republic of Korea; Department of Chemistry, Sungkyunkwan University, Suwon 16419, Republic of Korea.
E-mail addresses: jschang@krict.re.kr (J.-S. Chang), skyoon@korea.ac.kr (S.S. Yoon).
[1] These authors have contributed equally.

http://dx.doi.org/10.1016/j.jallcom.2017.06.190
0925-8388/

et al. [13] reported the fabrication of MIL-101(Cr) films by dip-coating a colloidal solution. Kusgens et al. [14] reported the water adsorption properties of CuBTC, ZIF-8, MIL-101, and MIL-100(Fe) nanoparticles, but did not present any attempt to create films of these materials.

Several techniques have been tested for MIL-100 film formation, including solvothermal methods [3,15], layer-by-layer deposition [16], electrochemical deposition [11,12], and dip coating [17]. However, these methods each have weaknesses. The solvothermal method requires multiple complex steps. Poor adhesion is a frequent issue with dip-coating. Electrochemical and layer-by-layer methods require conductive substrates [16]. In addition, films fabricated via these conventional methods do not have sufficiently high mechanical strength or stability for use in many real applications, where films must survive severe conditions.

Kim et al. [18] demonstrated the use of supersonic spraying to produce zeolitic imidazolate framework 8 (ZIF-8) films using a roll-to-roll process in open-air conditions. This method is rapid and scalable, with great potential for commercial viability. Supersonic spraying is not only high-throughput, but also produces highly dense, mechanically stable films. Simple one-step supersonic spraying permits the large-scale production of MOF films. Here, we demonstrate the use of supersonic spraying to fabricate MIL-100(Fe) films and examine the quality of the films by X-ray diffraction (XRD), Raman spectroscopy, Fourier transform infrared (FT-IR) spectroscopy, scanning electron microscopy (SEM), and atomic force microscopy (AFM). We measured the adhesion strength by testing scratchability of the MIL-100(Fe) films as well as their performance in nitrogen and water vapor adsorption. Water adsorption is important for application of MIL-100(Fe) in heat pumps, which utilize the storage and release of water vapor from porous materials in vapor-compression cycles [5,9,19]. The sensitivity of the fabricated film to its environment was also tested by measuring the electrical resistance changes in the fabricated films with changes in humidity.

2. Experimental procedures

2.1. MIL-100 precursor

MIL-100(Fe) was hydrothermally synthesized from a mixture containing iron nitrate ($Fe(NO_3)_3 \cdot 9H_2O$), 1,3,5-benzenetricarboxylic acid (BTC), and deionized water [20]. The molar composition of the reaction mixture was 1 Fe:0.67 BTC:55H_2O. The reactant mixture was loaded into a Teflon autoclave and stirred at room temperature for 30 min. The autoclave reactor was then heated to 160 °C and maintained at this temperature for 12 h. After the reaction, the product was cooled to room temperature, filtered and rinsed with deionized water and ethanol several times, and dried at 100 °C overnight.

2.2. Supersonic spraying

The MIL-100 films were prepared by a supersonic cold-spray process. A schematic of the cold-spray setup is shown in Fig. 1. The system is composed of a gas tank, gas heater, supersonic nozzle, ultrasonic atomizer, syringe pump, and $X-Y$ translation stage [21]. The coating solution is prepared by dispersing 1 g MIL-100 nanoparticles in 40 mL of DMF (dimethylformamide). A small amount (0.06 wt%) of polyacrylonitrile (PAN) was added to improve the dispersion of the MIL-100 nanoparticles in DMF. A syringe pump was used to inject the coating solution into a supersonic air stream produced using a converging-diverging nozzle. The exposure of the solution to a high-speed gas stream atomizes the dispersed MIL-100 particles and transports them to the substrate. The solution droplets evaporate rapidly and the suspended nanoparticles gain high kinetic energy from the hot compressed air. Their high-velocity impact yields well-adhered, compact MIL-100 films on the glass substrates. The substrates were installed on an X-Y translation stage that moves at a speed of ~35 mm/s. The gas velocity controls the impact speed and can be manipulated by altering the supersonic air pressure. In this study, the three "exit" gas velocities (V_e) used were 445, 600, and 664 m/s at the nozzle exit. The other operating conditions are given in Table 1.

2.3. Characterization

XRD patterns were obtained using a Rigaku SmartLab diffractometer with Cu Kα radiation ($\lambda = 0.15418$ nm) over a 2θ range of 3–25°. The surface morphologies were imaged using a high-resolution SEM (HR-SEM, S-5100, Hitachi Co., Japan) and an AFM (XE-100, Park Systems, Korea). Raman spectra were obtained with a Raman spectrometer (Horiba Jobin Yvon) using a 532 nm laser source. An FT-IR spectrometer (Spectrum GX, Perkin-Elmer) was used for chemical bonding analysis. The test sample for FTIR was prepared by mixing MIL100 with KBr. A Revetest Scratch Tester (RST, CSM Instruments, Switzerland) with a 100-μm diamond needle tip was used for scratch testing at a loading rate of 0.8 N/min and a table speed of 2 mm/min to check the adhesion of film. A scratch length of 12.5 mm was applied, giving the final load of 5 N. A nitrogen physisorption experiment was performed at −196 °C on a volumetric sorption analyzer (Micromeritics TriStar 3020) after dehydration of the sample at 150 °C for 12 h under high vacuum ($<1 \times 10^{-5}$ Torr). Water sorption isotherms were collected at 30 °C using a gravimetric sorption analyzer (IGA, Hiden Analytical Ltd.). The film was scratched to collect a powder of the coated sample.

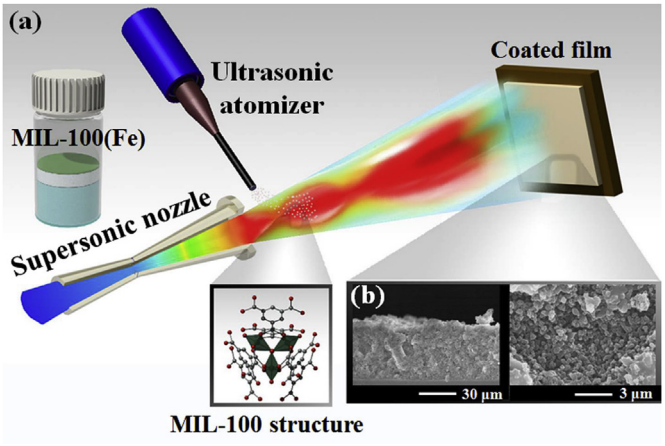

Fig. 1. (a) Schematic illustration of cold-spray process showing deposition of MIL-100 film (b) SEM cross-sectional view of the MIL-100 films. The color scale inside and outside the supersonic nozzle indicates the gas velocity. The flow accelerates from left (blue) to right (red) as the flow passes through the converging-diverging nozzle. (For interpretation of the references to colour in this figure legend, the reader is referred to the web version of this article.)

Table 1
Operating condition of supersonic spraying.

Spraying parameter	Values
Pressure (P_0) [bar]	2, 4, 6
Heater temperature [°C]	250
Flowrate [ml/min]	1.5
Traverse speed [mm/s]	35
Spraying distance [mm]	200
Number of layers	10

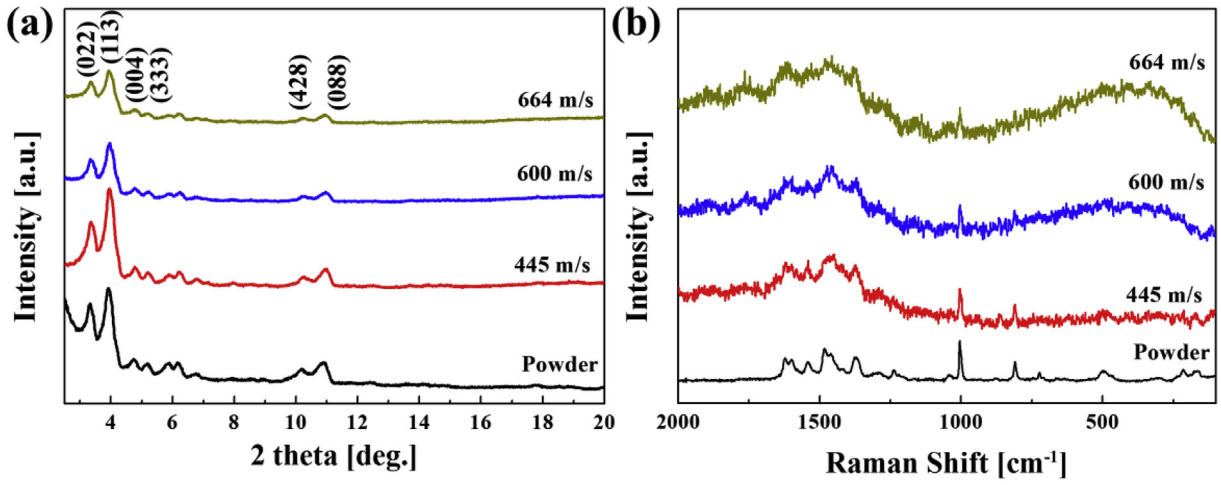

Fig. 2. (a) XRD patterns and (b) Raman spectra of powder and cold-sprayed MIL-100 films on glass substrates, deposited at the indicated gas velocities.

Samples of ~10 mg each were dehydrated at 150 °C for 5 h under high vacuum (<1 × 10^{-5} Torr) before adsorption.

2.4. Humidity sensing

The pristine MIL-100(Fe) film is highly resistive, so the resistance of the film was reduced by the addition of silver nanowire (AgNW) at a MIL-100:AgNW mass ratio of 1:0.015. For resistive sensing by the fabricated MIL-100/AgNW films, flat electrodes on each side were coated with silver paste to provide conducting interfaces with the measurement equipment. Initially, the resistances (R_0) of the films were measured at ambient temperature and relative humidity of 25 °C and 50%, respectively. The sensor films were then flushed inside an in-house developed controlled environmental chamber at constant relative humidity conditions of 60, 70, and 80%, before the resistance was measured again (R). Between successive introductions of the sensor films to humid conditions, recovery was performed by removing them from the chamber. The films were subjected to a fixed potential of 1 V and changes in the current carried by the sensor under exposure to various humidity conditions were recorded by a Keithley 2401 source meter. The sensor film resistance was calculated using Ohm's law.

3. Results and discussion

3.1. Material properties

The MIL-100 coated on a glass substrate (Fig. 2(a)) shows diffraction peaks at 3.4°, 3.9°, 4.9°, 5.3°, and 11°, corresponding to the (022), (113), (004), (333), and (428) planes of MIL-100, respectively [7,22]. The diffraction peaks of the films agree with those of the bulk powder, implying that the crystal structure of MIL-100 is maintained after cold-spray deposition at all of the tested gas velocities. No crystal deformation or additional Bragg peaks are observed in Fig. 2(a), demonstrating that variations in the cold-spray gas velocity do not influence the structural properties of films. We attribute this robustness to the rigidity of MIL-100 [23]. However, some amorphization is suggested by the diminished peak intensity in the pattern from the sample deposited at velocity V_e = 664 m/s. Also the grain size based on peak broadening decreased slightly from 48 nm to 45 nm as the velocity increases from 445 m/s to 664 m/s. In cold spraying, variations in gas pressure or temperature change the velocities of the suspended particles, affecting the kinetic energy dissipated upon impact with the substrate. As the impact velocity increased, the grain size tended to decrease and the surface roughness also decreased probably due to the intensified pulverization process at higher impact velocity, which in turn yields amorphization as the grain size decreases. However, high impact velocity promotes adhesion and formation of dense films. The low-velocity sample (V_e = 445 m/s) suffered from poor adhesion, but the adhesion of the V_e = 600 m/s film was much better, as discussed further below. Considering the effects of gas velocity, the samples deposited with the medium gas velocity of 600 m/s were selected for further morphological, mechanical, and gas and water adsorption testing. The sensor test sample was also deposited using 600 m/s gas velocity.

Fig. 2(b) depicts the Raman spectra of cold-sprayed MIL-100 films at different gas velocities. The spectra clearly show the vibration modes associated with the carboxylate groups from the benzenecarboxylate molecules of the organic linker. The bands at 1650 and 1285 cm^{-1} arise from the stretching of C=O and C–O bonds; in-plane peaks at 1614, 1445, 1176, and 1120 cm^{-1} are from complex vibrations from benzene rings; and out-of-plane deformation modes of C–H are observed at 827, 798, and 627 cm^{-1} [24].

The FT-IR spectra of the cold-sprayed MIL-100(Fe) films are shown in Fig. 3. The peaks at 710, 757, and 901 cm^{-1} belong to Fe–OH vibrations [25,26]. The peaks at 1375, 1454, and 1617 cm^{-1} arise from C=C and C=O vibrations, respectively, and are

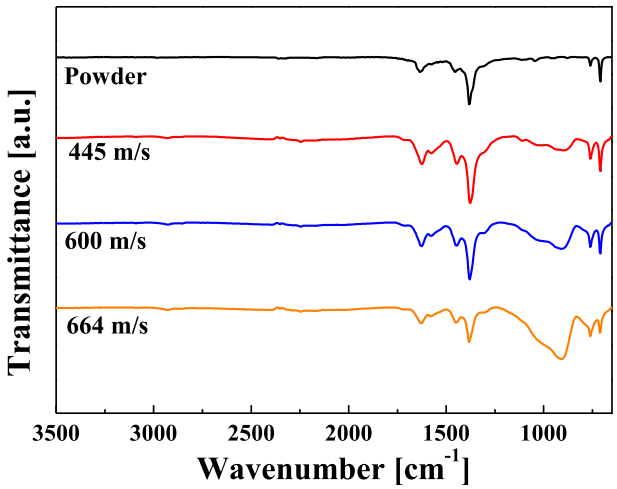

Fig. 3. FTIR spectra of velocity-dependent cold-sprayed MIL-100 films.

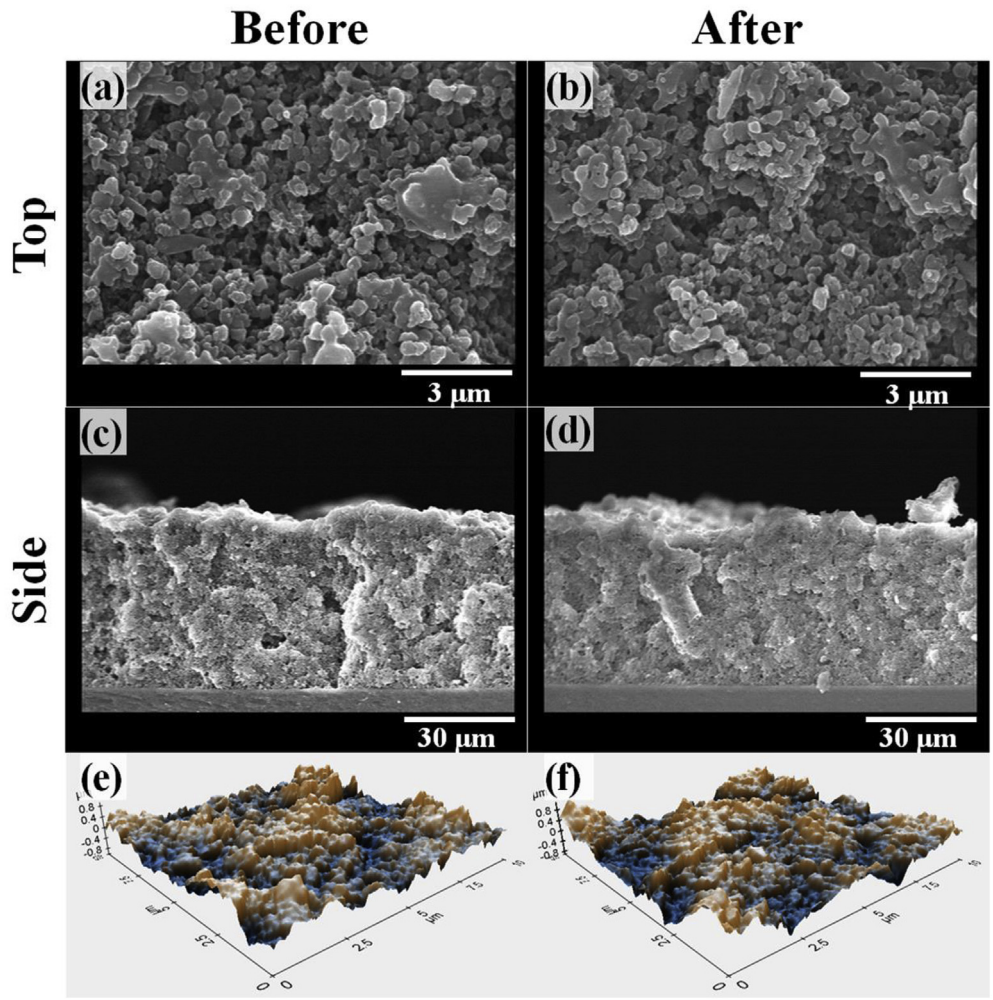

Fig. 4. Before sonication: (a) surface morphology and (c) cross-sectional view by SEM and (e) surface view by AFM. Similarly, after sonication test: (b) surface morphology and (d) cross-sectional view by SEM and (f) surface by AFM.

associated with the phenyl and carboxylate groups of BTC. Weak vibration bands appearing at 1710 cm^{-1} (ν_{as}(C═O)) and 1280 cm^{-1} (ν(C—O)) indicate the presence of only trace unreacted BTC [17]. The lowering of peak intensity between 1400 and 1700 cm^{-1} at higher speeds may be due to the loss of crystallinity and the amorphization of the framework, as suggested by the XRD patterns.

3.2. Mechanical properties

The SEM images of the cold-sprayed MIL-100 films show uniform, intact, and non-fractured films (Fig. 4(a)). To confirm adhesion, the films were sonicated in an ethanol solution for 10 min. After sonication, we observed no significant change in the morphology or thickness of the MIL-100 films, as shown in Fig. 4(b). The film thickness from the cross-sectional view was ~45 μm. The cross-sectional view also shows no effects of sonication, as seen in Fig. 4(c) and (d). The 3D AFM images of the MIL-100 film presented in Fig. 4(e) and (f) display peaks and valleys associated with the random stacking of MIL-100 particles in the film, confirming that no roughness change occurs after sonication.

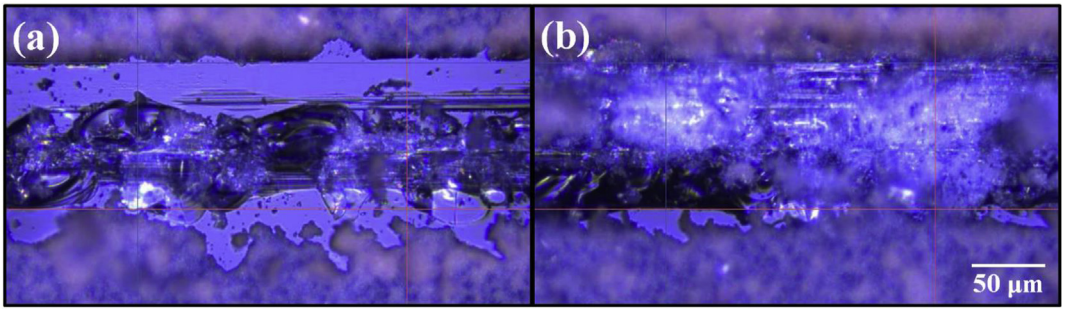

Fig. 5. Scratchability test of cold-sprayed MIL-100 films: (a) Start of scratch test and (b) end of scratch test. Sample film deposited with V_e = 600 m/s.

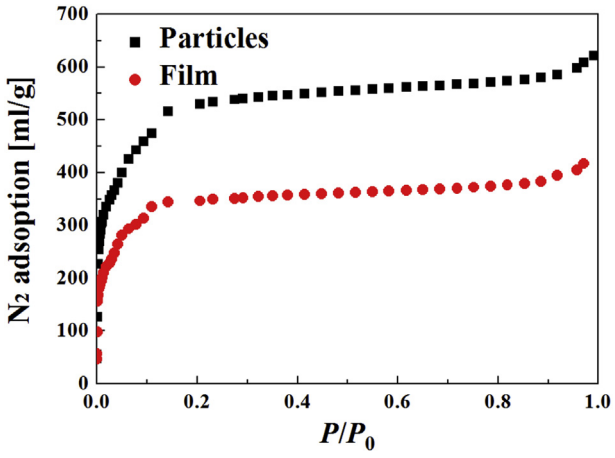

Fig. 6. N_2 adsorption isotherms of MIL-100 powder and cold-sprayed film.

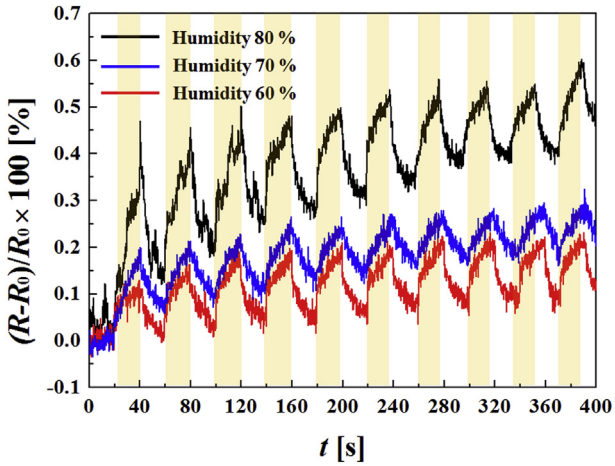

Fig. 8. Temporal response of cold-sprayed MIL-100/AgNW at different humidity conditions.

Table 2
BET results.

MOF type	S_{BET} [m^2 g^{-1}]	V_{Pore} [cm^3 g^{-1}]
Pure powder	2009	0.96
Film	1667	0.81

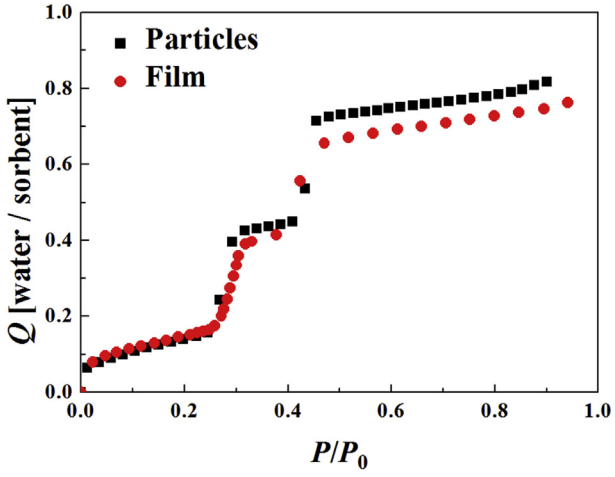

Fig. 7. Water adsorption isotherm of MIL-100 powder and cold-sprayed film.

Optical microscopy images of the cold-sprayed MIL-100 film before and after a peel-off scratchability test are shown in Fig. 5 for $V_e = 600$ m/s. The cohesion load (L_c) was ~1.04 N and adhesion load (L_a) ~ 1.84 N. The sample deposited with 445 m/s velocity could not be measured due to poor adhesion as it resulted in lower critical load than the minimum measurement limit of the equipment.

3.3. Gas and water adsorption

The specific surface areas of the MIL-100 powder and cold-sprayed film were obtained from N_2 adsorption isotherms (Fig. 6). Compared with the pristine MIL-100(Fe) powder, the cold-sprayed MIL-100(Fe) film exhibits a significant decrease in N_2 adsorption because some of its pores are blocked by the PAN used in the cold-spray process. Consequently, the BET surface area decreased from 2009 $m^2 \cdot g^{-1}$ to 1667 m^2 g^{-1} after cold-spraying.

The surface area observed in our cold-spray case is higher than that of the electrochemically synthesized films reported by Campagnol et al. [11]. Parameters such as the Brunauer–Emmett–Teller (BET) specific surface area (S_{BET}) and pore volume (V_{pore}) of the powder and cold-spray-coated sample are compiled in Table 2.

Water sorption studies of the pristine and cold-sprayed MIL-100 were performed at 30 °C after dehydration at 150 °C for 10 h (Fig. 7). MIL-100(Fe) possesses unique sorption properties, evidenced by the two-step isotherms for water vapor due to the capillary condensation steps in the mesoporous cages. Fig. 7 shows a slow rise in water adsorption for cold sprayed MIL-100 at lowest relative pressure ($P/P_0 = 0.2$). Water uptake rises suddenly with a step at $P/P_0 = 0.45$ that corresponds to the filling of 25 Å mesopores followed by 29 Å mesopores. The water adsorption is saturated at $P/P_0 = 0.5$ and further slight adsorption is due to the adsorption within interparticulate voids. MIL-100(Fe) is an industrially useful water sorbent because it has a high vapor sorption ability, structural stability, and sorption durability. As mentioned above, the cold-sprayed MIL-100(Fe) shows a smaller pore volume than the pristine powder because of the effects of the spraying process. Therefore, the water adsorption capacity is also decreased in comparison with pristine MIL-100(Fe). Our data agrees well with that reported by Jeremias et al. [27] and Kusgens et al. [14]. Table 3 compares the adsorption parameters of various MOF films used for gas and water adsorption applications. Compared to previously reported films, based on BET surface areas, the MIL-100(Fe) films in this work

Table 3
MIL films adsorption studies.

Film	Coating technique	Surface area [m^2 g^{-1}]	Application	Ref.
MIL-101	Dip coating	–	Water/vapor adsorption	[13], 2009
MIL-89	Chemical bath deposition	–	Water adsorption	[17], 2009
MIL-100	Dip coating	–	Water adsorption	[3], 2012
MIL-100	Electrochemical synthesis	722	Water/gas adsorption	[11], 2013
MIL-100	**Supersonic spraying**	**1667**	**Water/gas adsoption**	**Present**

have larger surface areas and therefore can be used for similar applications. Thus, the successful deposition of porous MIL-100 films by cold-spraying confirms that the cold-spray technique is viable for producing well-adhered, large-area MIL-100 films for applications such as gas and water adsorption.

The resistance across the MIL-100:AgNW film with changes in humidity was measured by a two-probe setup. To explore the cold-sprayed MIL-100 as a humidity sensor, dynamic testing of the MIL-100:AgNW films was performed at constant humidity. The response time for the absorption and desorption curves is shown in Fig. 8. The response time to a continuous humidity level of 60% is 20 s. The recovery time is similar at ~20 s. Notably, the MIL-100(Fe) coating also responds to very small changes in the humidity of ~10% difference. Further, testing after ten additional cycles demonstrates good reproducibility of the sensing behavior of the MIL-100 films. The response time is similar for humidity levels of 70% and 80%, but the response factor (R/R_0) is increased at 80% humidity. The response and recovery times are relatively short and similar for different humidity conditions; hence, the sensor using MIL-100 film can be regarded as a fast-response humidity sensor.

4. Conclusion

We demonstrate the fabrication of MIL-100(Fe) films by a simple and scalable supersonic spraying method for use in gas and water adsorption and sensing applications. The film exhibited a surface area of 1667 $m^2 g^{-1}$, comparable to that of the MIL-100(Fe) powder, indicating that film formation via supersonic spraying retained the original properties of the MIL-100(Fe) powder. A water adsorption test also confirmed that the adsorption capability of the film approached that of the dispersed powder. The film scratchability test showed mechanical stability sufficient for real commercial applications. The film's cyclic sensitivity to the environmental humidity level showed potential applications of the material as a water vapor sensor.

Acknowledgements

This research was supported by Global Frontier Program through the Global Frontier Hybrid Interface Materials (GFHIM) of the National Research Foundation of Korea (NRF) funded by the Ministry of Science, ICT & Future Planning (2013M3A6B1078879), NRF-2016M1A2A2936760, and NRF-2017R1A2B4005639.

References

[1] L.E. Kreno, K. Leong, O.K. Farha, M. Allendorf, R.P. Van Duyne, J.T. Hupp, Chem. Rev. 112 (2012) 1105–1125.
[2] J.-R. Li, Y. Ma, M.C. McCarthy, J. Sculley, J. Yu, H.-K. Jeong, P.B. Balbuena, H.-C. Zhou, Coord. Chem. Rev. 255 (2011) 1791–1823.
[3] A. García Márquez, A. Demessence, A.E. Platero-Prats, D. Heurtaux, P. Horcajada, C. Serre, J.S. Chang, G. Férey, V. de la Peña-O'Shea, C. Boissière, Eur. J. Inorg. Chem. 2012 (2012) 5165–5174.
[4] V. Stavila, A.A. Talin, M.D. Allendorf, Chem. Soc. Rev. 43 (2014) 5994–6010.
[5] S.K. Henninger, F. Jeremias, H. Kummer, C. Janiak, Eur. J. Inorg. Chem. 2012 (2012) 2625–2634.
[6] G. Férey, C. Mellot-Draznieks, C. Serre, F. Millange, J. Dutour, S. Surblé, I. Margiolaki, Science 309 (2005) 2040–2042.
[7] Y. Xu, L. Xu, S. Qi, Y. Dong, Z.u. Rahman, H. Chen, X. Chen, Anal. Chem. 85 (2013) 11369–11375.
[8] J.W. Yoon, Y.-K. Seo, Y.K. Hwang, J.-S. Chang, H. Leclerc, S. Wuttke, P. Bazin, A. Vimont, M. Daturi, E. Bloch, P.L. Llewellyn, C. Serre, P. Horcajada, J.-M. Grenèche, A.E. Rodrigues, G. Férey, Angew. Chem. Int. Ed. 49 (2010) 5949–5952.
[9] A. Cadiau, J.S. Lee, D. Damasceno Borges, P. Fabry, T. Devic, M.T. Wharmby, C. Martineau, D. Foucher, F. Taulelle, C.-H. Jun, Y.K. Hwang, N. Stock, M.F. De Lange, F. Kapteijn, J. Gascon, G. Maurin, J.-S. Chang, C. Serre, Adv. Mater. 27 (2015) 4775–4780.
[10] Y.-K. Seo, J.W. Yoon, J.S. Lee, Y.K. Hwang, C.-H. Jun, J.-S. Chang, S. Wuttke, P. Bazin, A. Vimont, M. Daturi, S. Bourrelly, P.L. Llewellyn, P. Horcajada, C. Serre, G. Férey, Adv. Mater. 24 (2012) 806–810.
[11] N. Campagnol, T. Van Assche, T. Boudewijns, J. Denayer, K. Binnemans, D. De Vos, J. Fransaer, J. Mater. Chem. A 1 (2013) 5827–5830.
[12] R. Ameloot, L. Stappers, J. Fransaer, L. Alaerts, B.F. Sels, D.E. De Vos, Chem. Mater. 21 (2009) 2580–2582.
[13] A. Demessence, P. Horcajada, C. Serre, C. Boissiere, D. Grosso, C. Sanchez, G. Ferey, Chem. Commun. (2009) 7149–7151.
[14] P. Küsgens, M. Rose, I. Senkovska, H. Fröde, A. Henschel, S. Siegle, S. Kaskel, Microporous Mesoporous Mater. 120 (2009) 325–330.
[15] Y.S. Li, H. Bux, A. Feldhoff, G.L. Li, W.S. Yang, J. Caro, Adv. Mater. 22 (2010) 3322–3326.
[16] O. Shekhah, J. Liu, R.A. Fischer, C. Wöll, Chem. Soc. Rev. 40 (2011) 1081–1106.
[17] P. Horcajada, C. Serre, D. Grosso, C. Boissiere, S. Perruchas, C. Sanchez, G. Férey, Adv. Mater. 21 (2009) 1931–1935.
[18] D.-Y. Kim, B.N. Joshi, J.-G. Lee, J.-H. Lee, J.S. Lee, Y.K. Hwang, J.-S. Chang, S. Al-Deyab, J.-C. Tan, S.S. Yoon, Chem. Eng. J. 295 (2016) 49–56.
[19] A. Freni, A. Frazzica, B. Dawoud, S. Chmielewski, L. Calabrese, L. Bonaccorsi, Appl. Therm. Eng. 50 (2013) 1658–1663.
[20] Y.-K. Seo, J.W. Yoon, J.S. Lee, U.H. Lee, Y.K. Hwang, C.-H. Jun, P. Horcajada, C. Serre, J.-S. Chang, Microporous Mesoporous Mater. 157 (2012) 137–145.
[21] D.Y. Kim, S. Sinha-Ray, J.J. Park, J.G. Lee, Y.H. Cha, S.H. Bae, J.H. Ahn, Y.C. Jung, S.M. Kim, A.L. Yarin, Adv. Func. Mater. 24 (2014) 4986–4995.
[22] C.-F. Zhang, L.-G. Qiu, F. Ke, Y.-J. Zhu, Y.-P. Yuan, G.-S. Xu, X. Jiang, J. Mater. Chem. A 1 (2013) 14329.
[23] P.D. Kolokathis, E. Pantatosaki, G.K. Papadopoulos, J. Phys. Chem. C 119 (2015) 20074–20084.
[24] S. Bordiga, C. Lamberti, G. Ricchiardi, L. Regli, F. Bonino, A. Damin, K.P. Lillerud, M. Bjorgen, A. Zecchina, Chem. Commun. (2004) 2300–2301.
[25] R. Liang, R. Chen, F. Jing, N. Qin, L. Wu, Dalton trans. 44 (2015) 18227–18236.
[26] M. Belkhedkar, A. Ubale, Int. J. Mater. Chem. 4 (2014) 109–116.
[27] F. Jeremias, A. Khutia, S.K. Henninger, C. Janiak, J. Mater. Chem. 22 (2012) 10148–10151.